The International Journal of Advanced Manufacturing Technology (2019) 101:1403–1421
https://doi.org/10.1007/s00170-018-2915-8

ORIGINAL ARTICLE

A new contouring error estimation for the high form accuracy of a multi-axis CNC machine tool

Jing Zhang[1] · Jiexiong Ding[1] · Qingzhao Li[1] · Zhong Jiang[1] · Qicheng Ding[1] · Li Du[1] · Wei Wang[1]

Received: 2 June 2018 / Accepted: 22 October 2018 / Published online: 20 November 2018

Abstract
The evaluation of contouring error is important for multi-axis CNC machines because the tolerance specifications of manufactured parts are directly affected by contouring error. One of the fundamental quality inspections to verify that a manufactured part meets the expected tolerance is via form error evaluations. However, the existing estimation methods of contouring error are based on the position tolerance requirements. To meet the form tolerance requirements for the parts, this paper focuses on developing a high-accuracy estimation method of contouring error that is not related to a datum (ND-contouring error). In the proposed estimation method, at first, the minimum zone tolerance (MZT) method is used to transform the ideal tool tip path to match the actual one. Subsequently, by comparing the position and orientation between the actual point and the nearest point on the transformed ideal tool path, the ND-contouring error and orientation contouring error of the tool can be estimated, respectively. In addition, the difference between the proposed estimation method and previous evaluation methods is comparatively analyzed. Finally, simulations and experiments are conducted by applying the S-shaped and B-shaped machining trajectories, respectively, and the results all verify the estimation accuracy of the ND-contouring error estimation method. By adoption of compensation based on the ND-contouring error estimation, the contouring error could be significantly reduced, which will improve the quality of parts.

Keywords Multi-axis CNC machine tools · Contouring error · Datum · Form error

1 Introduction

Multi-axis CNC machine tools have been extensively used to machine parts with sculptured surfaces in the fields of machinofacture and aerospace [1]. Due to the dynamic incompatibility among different axes, servo lag, nonlinearity, disturbance, and other factors [2], the contour accuracy of the machine tool is unsatisfactory. Many studies have focused on obtaining better contour tracking performance. Contouring error reduction methods in multi-axis CNC machining have been reviewed in reference [3]. The existing methods involve two major categories: tracking error control for single axis and contouring error control considering the coupling effect of each axis on the contour accuracy.

✉ Zhong Jiang
jiangzhong1989@163.com

[1] School of Mechanical and Electrical Engineering, University of Electronic Science and Technology of China, Chengdu 611731, China

Tracking error control is used to reduce the positioning error of each axis. Some methods, such as feed-forward tracking control (FFTC) [4], feed-forward friction observer (FFFO) [5], zero phase error tracking control (ZPETC) [6], and sliding mode control (SMC) [7], are studied to improve the tracking performance of each axis. Ideally, in the case where the tracking error of each axis is zero, there is no contouring error. However, it is impossible to obtain a perfect contour that is perfectly consistent with the ideal contour because of the limited bandwidth. In addition, R. Ramesh [8] has revealed that small contouring errors can still be obtained, even with significant tracking errors of each axis. Therefore, the contouring accuracy improvement should not focus only on the tracking control of each axis.

To obtain a better contouring accuracy, many researchers are dedicated to reducing the contouring error directly. In 1980, Koren [9] estimated the contouring error using the linearity of the tracking error of the driver and compensated the contour control signal of the speed loop of each axis using a cross-coupled controller (CCC). Since then, the information of multi-axis is comprehensively used to estimate and control

the contouring error. Most studies focused on the derivation of contouring error estimation algorithms because high-precision contouring error estimation is the prerequisite for improving the accuracy of the contour. There are two basic directions that may be followed to estimate the contouring error.

The first way is related to the tracking performance of the tool tip position; the current actual tool tip position and the corresponding ideal tool tip position are used to estimate the contouring error [10, 11]. Chung [12] proposed a method of tangent approximation to estimate the contouring error. Yang [13] calculated the contouring error of an arbitrary smooth path based on coordinate transformation and circular approximation. Lou [14] improved contouring accuracy using natural local approximation. Liu [15] derived the second-order Taylor approximation. Unlike the first contouring error estimation method, which is affected by the tracking performance, the second effort only needs the position information of the actual tool tip and ignores the position information of the corresponding ideal tool tip at the current moment [16].

The above contouring error estimation methods in Refs. [11–16] are directed to two-axis or three-axis machines without rotary axes. As we know, the rotation axis is the important factor to harm the accuracy of the tool tip position, which has a nonlinear relationship with the linear movement. After estimating the tool tip contouring error, the tool orientation error is calculated by using the linear approximation method [17]. Yang [18] obtained the online five-axis contouring error by calculating the distance from the point to the short line that represents the ideal tool tip trajectory and further improved to enhance the estimation accuracy [19]. The Ferguson curve approximation between discrete points is used to obtain the tool tip contouring error, and the tool orientation error is calculated by direct interpolation [20].

The ultimate goal of contouring error control is to improve the quality of part machining. The geometric error is an important index to evaluate the machining quality of machined parts. In the ISO/1101 standard, four kinds of geometrical tolerance are specified, namely, tolerances of form, orientation, location, and run-out. The form tolerances are not related to a datum, while the others are related to a datum. The previous contouring error is defined as the minimum distance between the actual point and the ideal tool path in a fixed coordinate system. The previous contouring error evaluation methods are related to a certain and constant datum and focus on the reduction of the position error of path to obtain a better position accuracy of parts. However, to our knowledge, the form error has not been considered alone to obtain a better form accuracy of parts.

The form error is an important fundamental quality characteristic to verify that a manufactured part meets the expected tolerances [21]. On the one hand, parts with form accuracy requirements have a wide range of applications in the manufacturing field. For example, in the fields of aerospace, parts with sculptured surfaces are widely used. For sculptured surface parts, the main item for evaluating the machining accuracy is the surface profile not related to a datum (ND-surface profile). On the other hand, it takes several processing steps to process a part from its original state to a finished product. The technological datum is a benchmark set during the machining process and can be divided into an assembly datum, a positioning datum, a measurement datum, and a process datum. Generally, in a multistage machining system, the technological datum is different in serious processing operations. For example, in the actual machining process, the machining datum of some parts may be cut off in the next process. Therefore, in some processes, we only need to ensure the form accuracy of the parts.

In this paper, a new estimation method of novel dynamic (ND)-contouring error is proposed for the machined workpiece with form error requirements. To distinguish from the definition of previous contouring error, ND-contouring error is defined in this paper. A nonlinear mathematical model for ND-contouring error evaluation is established based on the minimal zone condition. More precisely, first, tool tip path matching is used to evaluate the form error so that the actual tool path of the machining state up to the current time is close enough to its corresponding ideal tool tip path. Then, the shortest distance from the current actual tool tip position to the transformed ideal tool tip path is calculated, which is exactly the evaluation result. Finally, the proposed method is verified by simulations and experiments.

Unlike previous studies, the purpose of this paper is to guarantee the accuracy of the form of the tool tip path. Previous works are mainly dedicated to reducing the contouring error directly to obtain a better position accuracy of tool path. In this paper, to obtain better form accuracy of the tool path, the ND-contouring error is proposed to control the form error directly. Compared to the novelty of previous work, that of this paper includes the following:

(1) A high-accuracy estimation algorithm of multi-axis ND-contouring errors for parts with form tolerance requirement is proposed.
(2) The form-matching algorithm and the minimum zone method are applied in the estimation method to guarantee the accuracy of estimation.
(3) Based on the trajectory-independent information and universality of the homogenous transfer matrix (HTM) method, the proposed algorithm is adapted to different types of the machining trajectory and the machine tool.

The remainder of the paper is organized as follows. The definition of proposed ND-contouring error and the comparison of previous estimation is expounded in Section 2. Section 3 presents the matching algorithm and the ND-contouring error model. The simulations and experiments

are performed in Section 4. Finally, the conclusion is drawn in Section 5.

2 Advantages of the proposed ND-contouring error estimation

2.1 Assessment of manufactured sculptured surface parts

Without loss of generality, sculptured surface parts are used as our research object. The main item for evaluating the machining accuracy of complex surfaces is the ND-surface profile, which describes the difference between the measured actual surface and the ideal surface.

According to ISO/1101 [22], for the profile tolerance of a surface not related to a datum, the tolerance zone is limited by two surface enveloping spheres of diameter 2ξ, the centers of which are situated on a surface having the theoretically exact geometrical form. As shown in Fig. 1, the actual surface is limited by the two surfaces (top deviation surface and bottom deviation surface in Fig. 1). The central surface formed by the centers of these spheres is located between the top and bottom deviation surfaces. The center surface has the same geometrical form as the ideal surface.

There are two key problems in solving the ND-surface profile error evaluation of sculptured surface parts. One problem is the registration of the center surface. The other problem is to find the closest points on the ideal model that correspond to measured actual points. Many researchers have developed the free-form surface-matching problem. Least squares method (LSM) [23] and minimum zone tolerance (MZT) [24] are the two common methods in the literature, and many optimization algorithms are proposed to optimize the model to achieve the optimal matching [21, 25]. LSM is one of the common methods because it is easy to compute. However, the LSM cannot guarantee the minimum zone solution specified in the ISO/1101 standard and ASME_Y14.5.1M-1994 [26]. According to the ASME_Y14.5.1M-1994 (the industry standard), when assessing the form error of workpiece, the position of the fitting element should meet the principle of the minimum conditions; that is, the measured maximum factor of the actual element is the smallest. This outcome can result in the overestimation of form tolerances and erroneous disposal of the workpiece. To improve the estimation accuracy, the MZT is used in this paper. The MZT to assess the ND-surface profile error refers to the minimum distance between the top deviation surface and bottom deviation surface, which is essentially a nonlinear optimization problem.

According to the definition of ND-surface profile, three mathematical models to evaluate the ND-surface profile error are given as follows:

$$\begin{aligned} way1 &: \min\{\max[F(U,X)]-\min[F(U,X)]\}, \\ way2 &: \min\{\max[F(U,X)]\}, \\ way3 &: \max\{\min[F(U,X)]\}, \end{aligned} \tag{1}$$

where U is the ideal feature parameter set, and X is the actual feature parameter set. The second way is used to establish the mathematical model for evaluating the ND-surface profile error to meet the standard definition of the profile error as reported in ISO/1101.

The measurement surface is represented by a limited number of measurement points, and each measurement point in the design surface has a unique corresponding ideal point which is nearest to the measured actual one. The measurement point and the ideal point combine the measurement point set and the theoretical point set, respectively. Obviously, the measurement points and the corresponding ideal points will form point

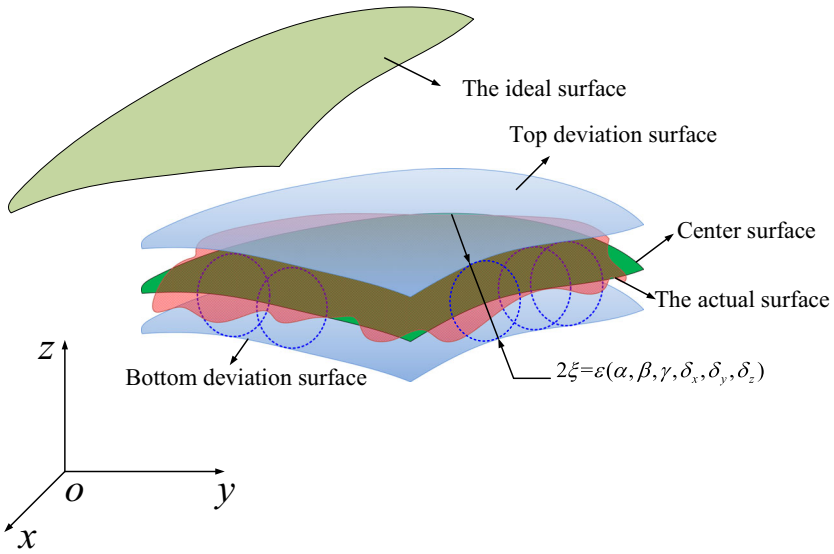

Fig. 1 Surface profile tolerances

pairs. The matching transformation is obtained by minimizing the maximum distances of the collective point-to-point.

$$error(U) = \min[2\max(d_i | i = 1, 2, ..., n)] \quad (2)$$

The target element d_i, which is the distance from the measuring point to the ideal surface profile, is used to evaluate the model.

The distance from the measuring point to the surface to be measured can be expressed as the Euclidean distance between two points of the point pair.

$$d(p, S) = \|p - q\|_2 \quad (3)$$

where p is any point in the set of measurement points, q is any point in the set of ideal points, and S is the measured surface.

According to the definition of free-form surface profile tolerance in ASME and ISO/1101, combined with the above distance function, the measuring point inside the tolerance zone should satisfy the following formula:

$$|d(p, S)| \leq \xi \quad (4)$$

2.2 Comparison between the proposed ND-contouring error and previous contouring error

It is obvious that the tool tip position of a machine tool and the point position of workpiece could be mapped with each other. Therefore, we transform the improvement of the workpiece machining quality into the reduction of the form error of the tool path. In the ISO/1101 standard [22], for the profile tolerance of a line not related to a datum, the tolerance zone is limited by two lines enveloping circles of diameter 2ξ, the centers of which are situated on a line (*centerline* in Fig. 2) having the theoretically the exact geometrical form. As shown in Fig. 2, the *centerline* has the same form as the ideal tool path. The radius of the circles is ξ, and the form error of the actual tool path is 2ξ. The value of 2ξ is related to the location of the *centerline*, and the location of *centerline* can be represented by the three translation parameters (δ_x, δ_y, δ_z) and three rotation parameters (α, β, γ). In Fig. 2, the difference between previous contouring error and the proposed ND-contouring error is illustrated. The definition of the proposed ND-contouring error is the minimum distance $\overrightarrow{P_aP_c}$ between the actual point P_a and the *centerline* when the *centerline* is under the condition that the value of 2ξ is the smallest, while the previous contouring error $\overrightarrow{P_aP_i}$ is the minimum distance between the actual point P_a and the ideal tool path in a fixed coordinate system.

As shown in Fig. 3, an example is given to explain the definition of the proposed ND-contouring error more clearly. The processing status up to the current moment is represented by the curve $P_{a_0}P_{a_\tau}$. Note that the actual tool tip path $P_{a_o}P_{a_\tau}$ and the ideal tool tip path $P_{i_o}P_{i_\tau}$ have the same geometrical form. As mentioned above, previous studies on the contouring error algorithm focused on obtaining the high-precision ε value as shown in Fig. 3a, where ε is the minimum distance between the current actual point P_{a_τ} and the ideal tool tip path in the given coordinate system. However, when the actual tool tip path and the "centerline" completely coincide with each other, the radius ξ of the circles is zero. Thus, the form error of the actual tool tip path $P_{a_o}P_{a_\tau}$ is zero. Therefore, unlike

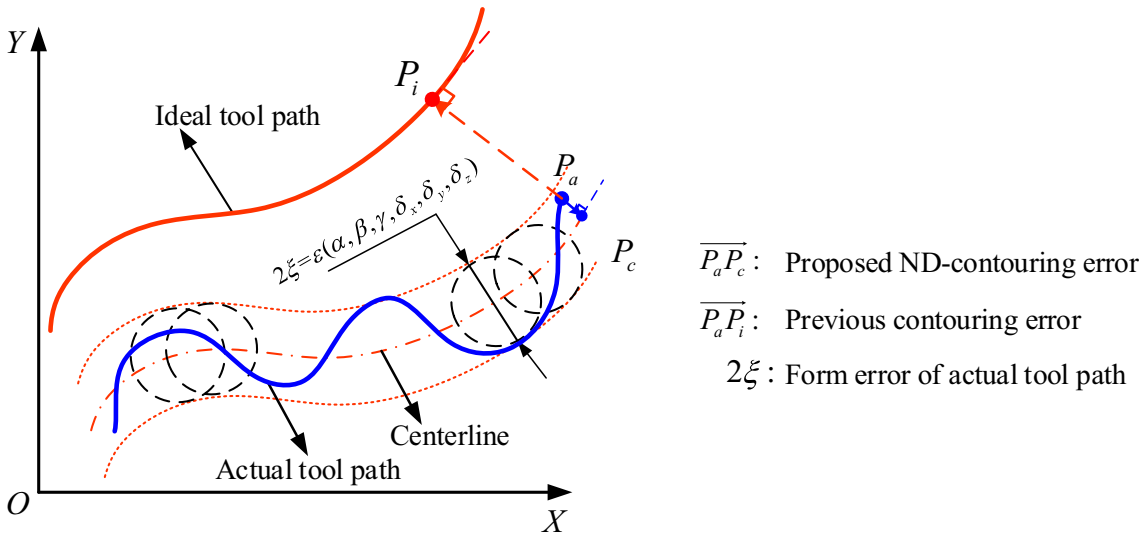

Fig. 2 The definition of the proposed ND-contouring error

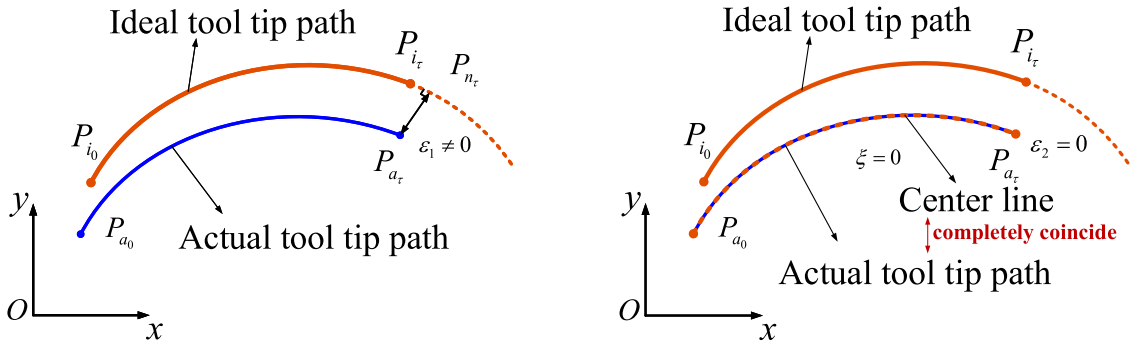

(a) Previous contouring error estimation (b) Proposed contouring error estimation

Fig. 3 The different error value of two estimation methods. **a** Previous contouring error estimation. **b** Proposed contouring error estimation

the conventional method considering the error value as $\varepsilon_1(\varepsilon_1 \neq 0)$, the proposed ND-contouring error is zero $\varepsilon_2(\varepsilon_2 = 0)$ as shown in Fig. 3b.

According to the above analysis, the contouring errors are estimated differently by the two different methods. Obtaining a high-accuracy estimation of contouring error is crucial to improving the machining accuracy. To show the advantages of the proposed contouring error, the form error of the compensated tool tip path based on the two different estimated contouring errors is compared. Assuming that the estimated error can be fully compensated in the next process of machining, the two error estimation methods in Fig. 3 will form two different compensated actual tool tip paths. As shown in Fig. 4, the compensated actual tool tip path is indicated by the solid blue line. It is obvious that the form error of the actual tool tip path in Fig. 4a is larger than that in Fig. 4b. This outcome demonstrates that the previous estimation does not necessarily guarantee contouring accuracy for the objects with form error requirements. Thus, the ND-contouring error has an advantage in obtaining a better form accuracy.

3 Estimation algorithm of ND-contouring error

3.1 Point-set matching for the registration of free-form tool tip path curves

Based on the ND-surface profile error estimation, the MZT is used in this paper to evaluate the tool path form error. According to the definition of the ND-contouring error, the ideal tool tip path should be matched to the actual tool tip path to evaluate the ND-contouring error. First, the ideal tool tip points are densified by NURBS curve interpolation. The ideal tool tip path C' is described in NURBS with parameter u, which is defined by the following form.

$$C'(u) = \frac{\sum_{j=0}^{n} Q_{i_j} w_j N_{j,p}(u)}{\sum_{j=0}^{n} w_j N_{j,p}(u)} = \sum_{j=0}^{n} Q_{i_j} R_{j,p}(u) \tag{5}$$

$$R_{j,p}(u) = \frac{w_j N_{j,p}(u)}{\sum_{k=0}^{n} w_k N_{k,p}(u)} \tag{6}$$

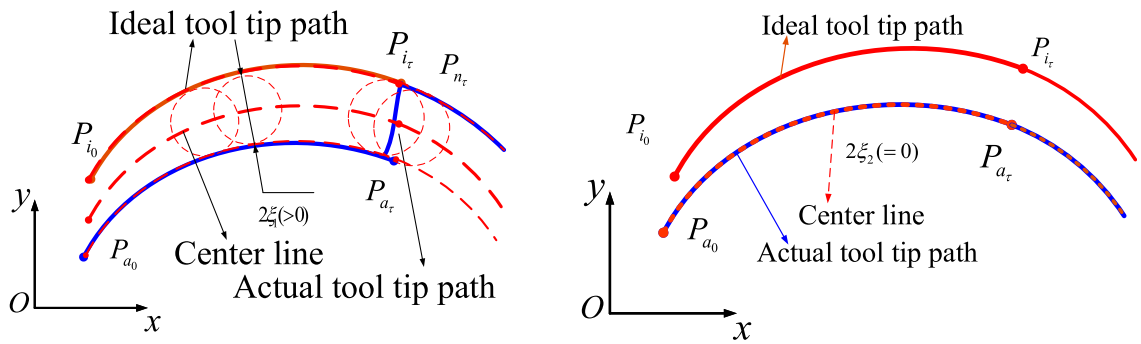

(a) Previous contouring error estimation (b) Proposed contouring error estimation

Fig. 4 The different actual tool tip paths of two estimation methods. **a** Previous contouring error estimation. **b** Proposed contouring error estimation

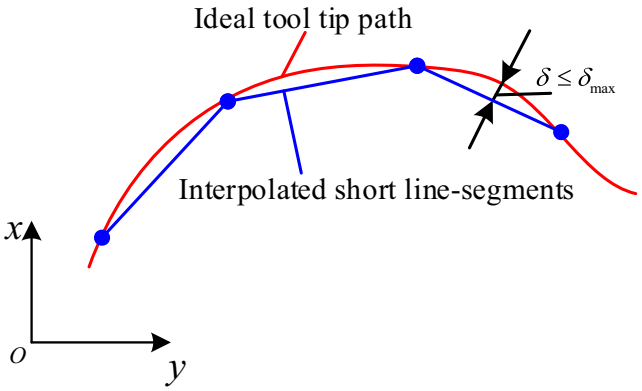

Fig. 5 Illustration of the line segment approximation

where Q_{i_j} represents the set of control points, w_j represents the weight, and $N_{j,\,p}(u)$ represents the normalized B-spline basis function of degree p.

As shown in Fig. 5, δ represents the chord error. $\delta_{\max}$ represents the preset chord error tolerance. During the interpolation process, the discrepancy between the interpolated short line segments and the ideal tool tip path will not exceed the preset chord error tolerance $\delta_{\max}$, which is typically set as 1 or less than 1 μm [27–29].

In our case, $C^{'}$ is obtained as a set of ideal tool tip points $P_{ij}(j=1,\ldots,n)$. For each actual point P_a, the corresponding closest point can be found in set $C^{'}$. Assuming $P_{i_j}^{'}$ $(j=0,\ldots,n)$ is the closest point found on the ideal tool tip path corresponding to actual tool tip point $P_{a_j}(j=0,\ldots,n)$, the distance $d\left(P_{a_j},C^{'}\right)$ between the actual tool tip point P_{a_j} and the ideal tool tip path $C^{'}$ is defined by reference to Section 2.1. By this definition, we have

$$\begin{aligned} d\left(P_{a_j},C^{'}\right) &= \min_{P_{i_k}^{'}\in C^{'},k\in\{0,\ldots,m\}} d(P_a,P_{ik}) \\ &= d\left(P_{a_j},P_{i_j}^{'}\right)_{P_{i_j}^{'}\in C^{'},j\in\{0,\ldots,n\}} \\ &= \sqrt{\left(x_{i_j}^{'}-x_{a_j}\right)^2+\left(y_{i_j}^{'}-y_{a_j}\right)^2+\left(z_{i_j}^{'}-z_{a_j}\right)^2} \end{aligned} \quad (7)$$

where $d\left(P_{a_j},C^{'}\right)$ is the Euclidean distance between the two points $P_{a_j}\left(x_{a_j},y_{a_j},z_{a_j}\right)$ and $P_{ij}^{'}\left(x_{i_j}^{'},y_{i_j}^{'},z_{i_j}^{'}\right)$.

$$P_{ij}^{'}=\left(x_{i_j}^{'},y_{i_j}^{'},z_{i_j}^{'}\right)=\mathrm{argmin}_{P_{ik}^{'}\in C^{'},k=0,\ldots,m} d\left(P_a,P_{ik}^{'}\right),j=0,\ldots,n \quad (8)$$

The two objects, actual tool path and ideal tool path, are represented by a set of 3-D points, which are considered the samples of a curve. The actual tool tip path is represented by a limited number of actual tool tip points $P_{a_j}(j=0,\ldots,n)$, which are obtained by sampling, and each actual tool tip point in the ideal tool tip path has a unique corresponding closest point.

The matching process is shown in Fig. 6. In the matching process of the current sampling time τ, the MZT algorithm is employed. First, the position of the actual tool tip path point cloud $\{P_{a_0},P_{a_1},\cdots,P_{a_\tau}\}$ and the corresponding closest points $\left(P_{i_0}^{'},P_{i_1}^{'},\ldots,P_{i_\tau}^{'}\right)$ in the ideal tool tip path are obtained in workpiece coordinate as shown in Fig. 6a. The location of the "centerline" in Section 2.2 can be obtained by transferring the ideal tool tip path. Thus, the point clouds $\left(P_{i_0}^{'},P_{i_1}^{'},\ldots,P_{i_\tau}^{'}\right)$ are moved to approach the actual $\{P_{a_0},P_{a_1},\cdots,P_{a_\tau}\}$ by minimizing the maximum distance between two point clouds to meet the minimum zone solution specified in ISO/1101 standard. Subsequently, the ideal point clouds $\left(P_{i_0}^{'},P_{i_1}^{'},\ldots,P_{i_\tau}^{'}\right)$ are rotated and transferred as rigid body transformation by using rotation matrix $R^{(\tau)}$ and translation matrix $T^{(\tau)}$ to further approach the actual $\{P_{a_0},P_{a_1},\cdots,P_{a_\tau}\}$ as shown in Fig. 6b.

Assuming $P_t{}^{(\tau)}=\left\{P_{t_j}{}^{(\tau)}=\left(x_{t_j}{}^{(\tau)},y_{t_j}{}^{(\tau)},z_{t_j}{}^{(\tau)}\right)|j=1,2,\ldots,\tau\right\}$ is the transformed ideal tool tip point set corresponding to the ideal tool tip point set $P_i{}^{(\tau)}=\left\{P_{i_0}{}^{'},P_{i_1}{}^{'},\ldots,P_{i_\tau}{}^{'}\right\}$, we can get:

$$P_\tau\left(\psi_\alpha^{(\tau)},\psi_\beta^{(\tau)},\psi_\gamma^{(\tau)},\xi_x^{(\tau)},\xi_y^{(\tau)},\xi_z^{(\tau)}\right)=P_i{}^{(\tau)}\begin{bmatrix}R^{(\tau)} & T^{(\tau)}\\ 0 & 1\end{bmatrix} \quad (9)$$

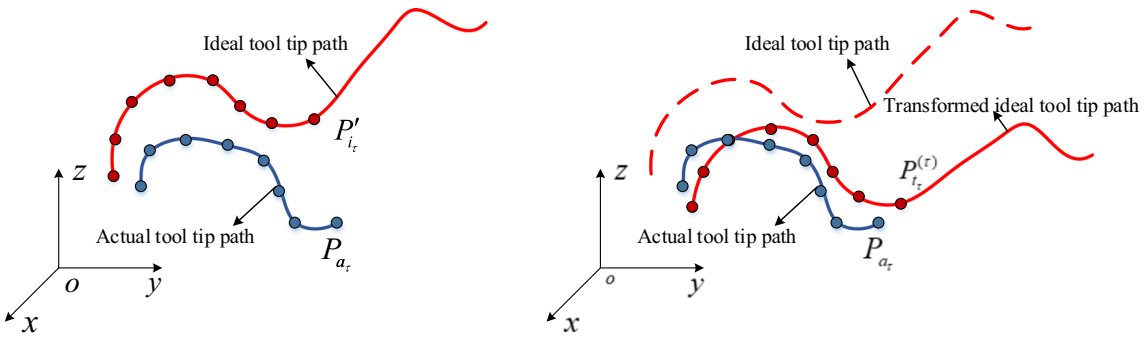

(a) initial postures (b) minimizing the maximum distance

Fig. 6 The matching process of actual tool tip path points to the ideal tool tip path. **a** Initial postures. **b** Minimizing the maximum distance

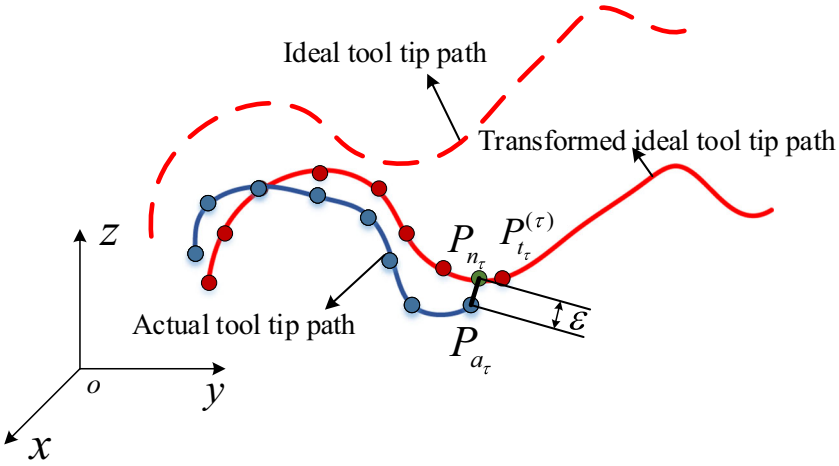

Fig. 7 Calculate ND-contouring error

where $\psi_\alpha^{(\tau)}$, $\psi_\beta^{(\tau)}$, and $\psi_\gamma^{(\tau)}$ are the rotation angles of the actual tool tip path along the x, y, and z axes, respectively; and $\xi_x^{(\tau)}$, $\xi_y^{(\tau)}$, and $\xi_z^{(\tau)}$ are the translations in the x, y, and z directions, respectively.

$$T^{(\tau)} = \left[\xi_x^{(\tau)}, \xi_y^{(\tau)}, \xi_z^{(\tau)}\right]^T \tag{10}$$

$$R^{(\tau)} = \begin{bmatrix} \cos\psi_\beta^{(\tau)}\cos\psi_\gamma^{(\tau)} & \sin\psi_\alpha^{(\tau)}\sin\psi_\beta^{(\tau)}\cos\psi_\gamma^{(\tau)} - \cos\psi_\alpha^{(\tau)}\sin\psi_\gamma^{(\tau)} & \cos\psi_\alpha^{(\tau)}\sin\psi_\beta^{(\tau)}\cos\psi_\gamma^{(\tau)} + \sin\psi_\alpha^{(\tau)}\sin\psi_\gamma^{(\tau)} \\ \cos\psi_\beta^{(\tau)}\sin\psi_\gamma^{(\tau)} & \sin\psi_\alpha^{(\tau)}\sin\psi_\beta^{(\tau)}\sin\psi_\gamma^{(\tau)} + \cos\psi_\alpha^{(\tau)}\cos\psi_\gamma^{(\tau)} & \cos\psi_\alpha^{(\tau)}\sin\psi_\beta^{(\tau)}\sin\psi_\gamma^{(\tau)} + \sin\psi_\alpha^{(\tau)}\cos\psi_\gamma^{(\tau)} \\ -\sin\psi_\beta^{(\tau)} & \sin\psi_\alpha^{(\tau)}\cos\psi_\beta^{(\tau)} & \cos\psi_\alpha^{(\tau)}\cos\psi_\beta^{(\tau)} \end{bmatrix} \tag{11}$$

The relationship between the ideal tool tip path and the transformed ideal tip tool path used for comparison is usually represented by the transformation matrix ($M^{(\tau)}$), which is defined as follows [30].

$$M^{(\tau)}\left(\psi_\alpha^{(\tau)}, \psi_\beta^{(\tau)}, \psi_\gamma^{(\tau)}, \xi_x^{(\tau)}, \xi_y^{(\tau)}, \xi_z^{(\tau)}\right) = \begin{bmatrix} R^{(\tau)} & T^{(\tau)} \\ 0 & 1 \end{bmatrix} \tag{12}$$

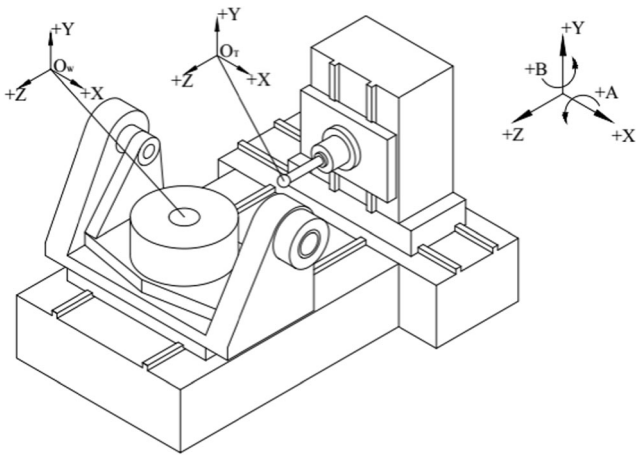

Fig. 8 Kinematics structure of the simulation and experiment

The objective function is set up using the second method mentioned in Section 2.1. In other words, the six parameters relative to the surface pose are optimized by the objective function.

$$\begin{aligned} &\mathrm{Min}\left[F\left(M^{(\tau)}\right)\right] \\ &= \mathrm{Min}\left[max_{j=0,\ldots,\tau} 2d_j\left(\psi_\alpha^{(\tau)}, \psi_\beta^{(\tau)}, \psi_\gamma^{(\tau)}, \xi_x^{(\tau)}, \xi_y^{(\tau)}, \xi_z^{(\tau)}\right)\right\}\Big] \end{aligned} \tag{13}$$

Based on the evaluation of ND-surface profile, the points on the actual tool path and the points on the ideal path should be matched, and the matching transformation is calculated by minimizing the maximum distances of the collective point-to-point. The goal of path matching is to make the ideal path close enough to the actual path. Therefore, at the current time τ, the objective function F is defined as the maximum distance between two point clouds:

$$\begin{aligned} &\mathrm{Min}\left[F\left(M^{(\tau)}\right)\right] = \mathrm{Min}\left\{max_{j=0,\ldots,\tau}\left\|P_{t_j}{}^{(\tau)} - P_{a_j}\right\|\right\} \\ &= \mathrm{Min}\left\{max_{j=0,\ldots,\tau}\left[\sqrt{\left(x_{t_j}{}^{(\tau)} - x_{a_j}\right)^2 + \left(y_{t_j}{}^{(\tau)} - y_{a_j}\right)^2 + \left(z_{t_j}{}^{(\tau)} - z_{a_j}\right)^2}\right]\right\} \end{aligned} \tag{14}$$

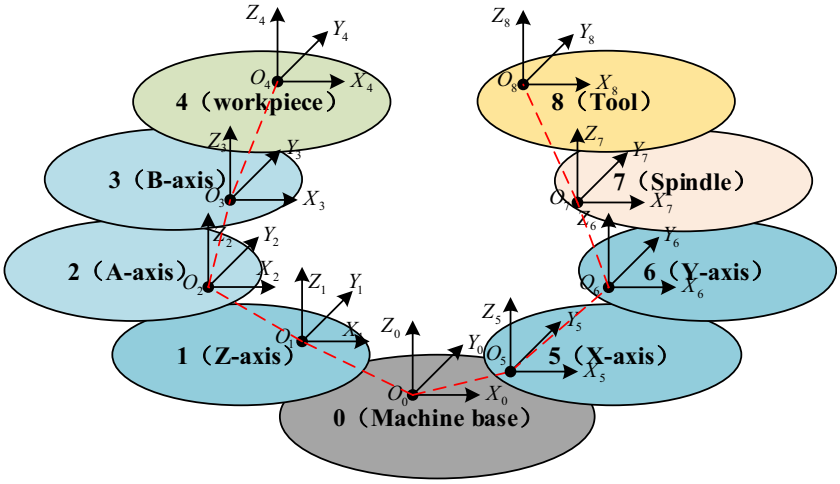

Fig. 9 The coordinate system structural diagram

Here, $P_{t_j}{}^{(\tau)}\left(x_{t_j}{}^{(\tau)}, y_{t_j}{}^{(\tau)}, z_{t_j}{}^{(\tau)}\right)$ and $P_{a_j}\left(x_{a_j}, y_{a_j}, z_{a_j}\right)$ are the transformed ideal tool tip points and actual tool tip points, respectively. The symbols $*_j$ and $*^{(\tau)}$ mean the variables * at time j and τ, respectively. Min[$*$] denotes the minimum function.

Following this, we can obtain the transformation matrix ($M^{(\tau)}$).

$$M^{(\tau)} = \text{argMin}\left\{ \max_{j=1}^{\tau} \left\| M^{(\tau)} P_{t_j}^{(\tau)} - P_{a_j} \right\| \right\} \tag{15}$$

3.2 Estimation of new contouring error

Once the ideal tool path is located, the ND-contouring error can be obtained by calculating the minimum distance of the actual tool tip and the transformed ideal tool tip path. As shown in Fig. 7, point P_{n_τ} is the closest point to the actual tool tip P_{a_τ} on the transformed ideal tool tip path, and the ND-contouring error is ε.

The multi-axis contouring error consists of several drive axis tracking errors based on the structure of the machine tool. Without the loss of generality, we take the type of five-axis machine tool with a tilting rotary table (Fig. 8) as an example for discussion. The forward kinematics describe the tool pose in the workpiece frame $\left(P_{i_j}, O_{i_j}\right)_{j=0,\ldots,n}$ as a motion command function to the five drivers of the machine $D_{i_j}\left(X_{i_j}, Y_{i_j}, Z_{i_j}, A_{i_j}, B_{i_j}\right)_{j=0,\ldots,n}$.

Assuming the machine tool has zero geometric errors, the tool forming point and the workpiece forming point will completely overlap. According to the relationship described in Fig. 9, $T_{bT}P_T = T_{bw}P_w$ can be obtained. Here, $P_T = (0\ \ 0\ \ -L\ \ 1)^T$ are the coordinates of the tool forming point in the tool coordinate system, and L is the distance from the tool tip point to the center of rotation. $T_{bT} = \prod_{t=n,L^n(8)=0}^{t=1} T_{L^t(8)L^{t-1}(8)}$ and $T_{bw} = \prod_{u=n,L^n(4)=0}^{u=1} T_{L^u(4)L^{u-1}(4)}$ are the homogenous transformation matrices of the tool chain and the workpiece chain, respectively.

The coordinates of the workpiece forming point in the workpiece coordinate system can be written as follows:

$$P_w = \left[\prod_{u=n,L^n(4)=0}^{u=1} T_{L^u(4)L^{u-1}(4)} \right]^{-1} \left[\prod_{t=n,L^n(8)=0}^{t=1} T_{L^t(8)L^{t-1}(8)} \right] \cdot P_T \tag{16}$$

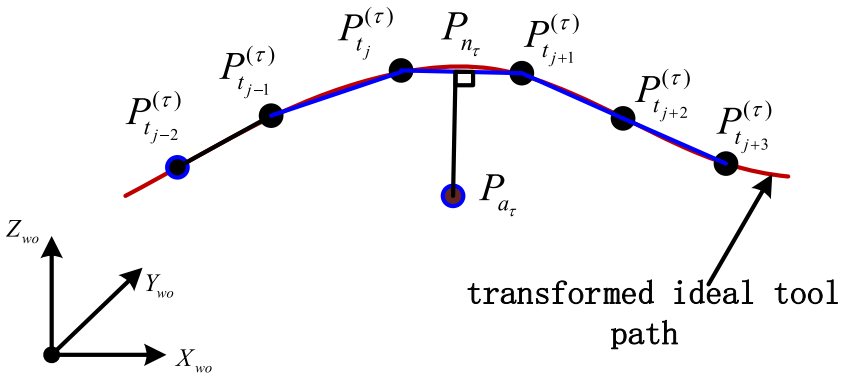

Fig. 10 Illustration of the ND-contouring error estimation

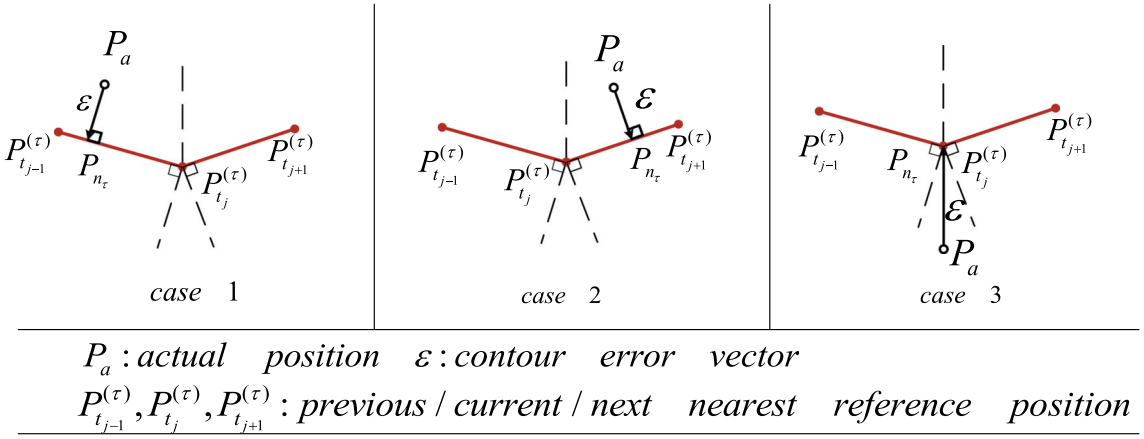

Fig. 11 Three possible cases in discrete calculation of contouring error [18]

$$T_{a01}=\begin{bmatrix}1&0&0&0\\0&1&0&0\\0&0&1&Z_a\\0&0&0&1\end{bmatrix},T_{a12}=\begin{bmatrix}1&0&0&0\\0&\cos A_a&-\sin A_a&0\\0&\sin A_a&\cos A_a&0\\0&0&0&1\end{bmatrix},T_{a23}=\begin{bmatrix}\cos B_a&0&\sin B_a&0\\0&1&0&0\\-\sin B_a&0&\cos B_a&0\\0&0&0&1\end{bmatrix},T_{a34}=\begin{bmatrix}1&0&0&x_{aw}\\0&1&0&y_{aw}\\0&0&1&z_{aw}\\0&0&0&1\end{bmatrix}$$

$$T_{a05}=\begin{bmatrix}1&0&0&X_a\\0&1&0&0\\0&0&1&0\\0&0&0&1\end{bmatrix},T_{a56}=\begin{bmatrix}1&0&0&0\\0&1&0&Y_a\\0&0&1&0\\0&0&0&1\end{bmatrix},T_{a67}=\begin{bmatrix}\cos\varphi_a&-\sin\varphi_a&0&0\\\sin\varphi_a&\cos\varphi_a&0&0\\0&0&1&0\\0&0&0&1\end{bmatrix},T_{a78}=\begin{bmatrix}1&0&0&x_{at}\\0&1&0&y_{at}\\0&0&1&z_{at}\\0&0&0&1\end{bmatrix}$$

The ideal input commands for each driver, after the drive system, are converted to the actual positions of each axis $D_{a_j}\left(X_{a_j},Y_{a_j},Z_{a_j},A_{a_j},B_{a_j}\right)$. Then, the position of an actual tool point $P_{a_j}\left(x_{a_j},y_{a_j},z_{a_j}\right)$ in the workpiece coordinate system is obtained by homogenous transfer matrix method [18].

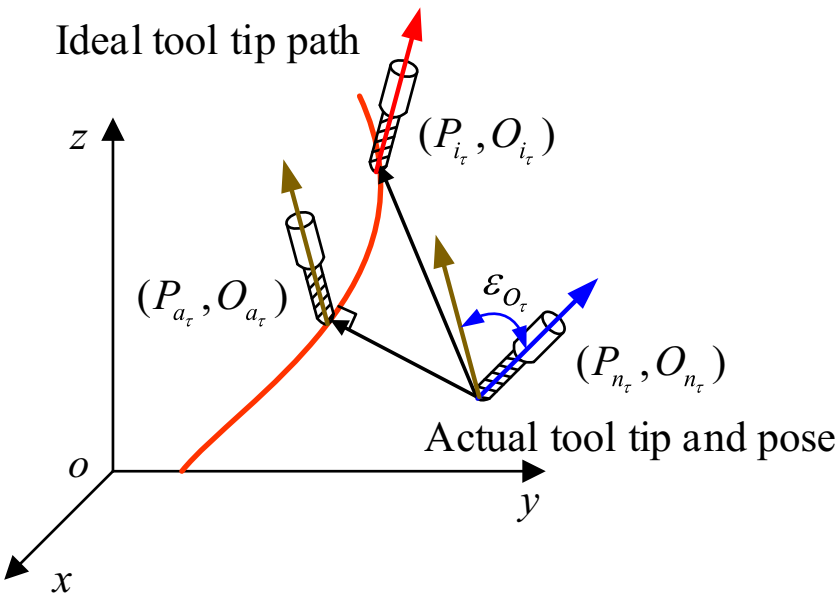

Fig. 12 The definition of tool orientation contouring errors

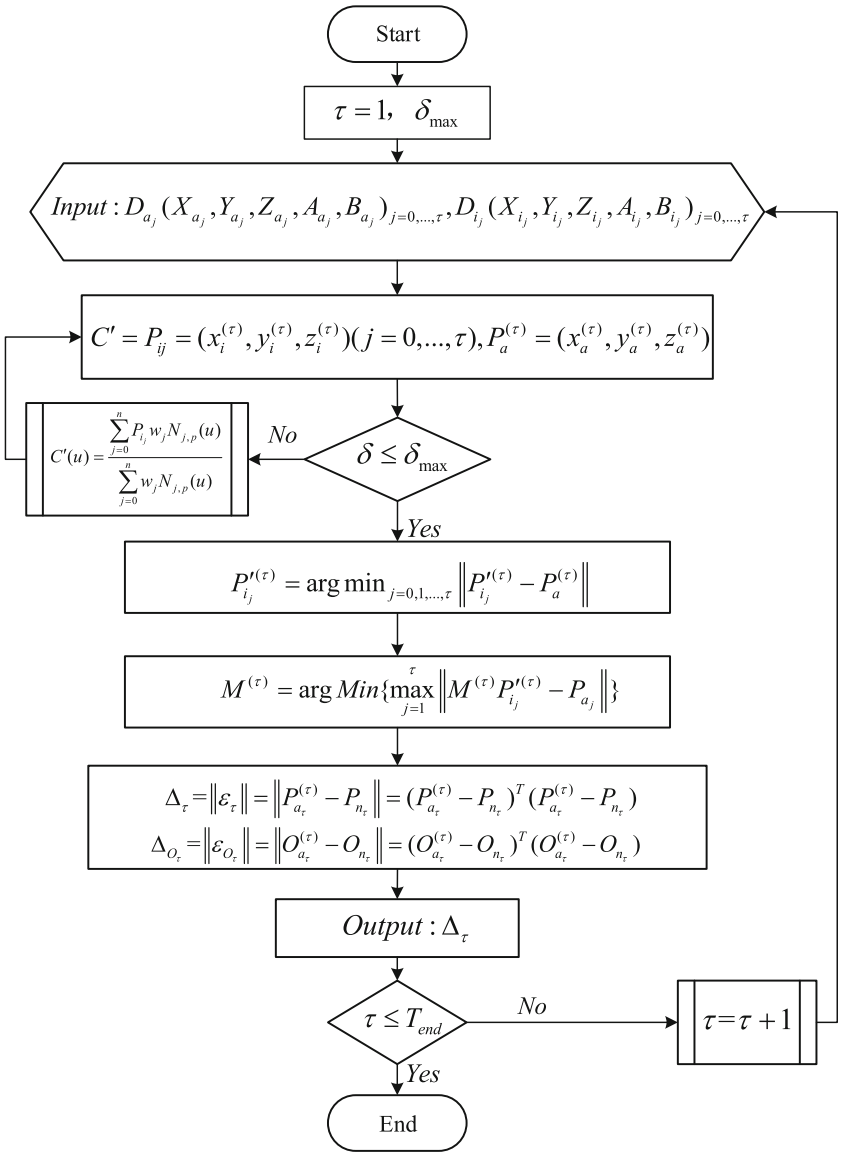

Fig. 13 Flowchart of the ND-contouring error estimation algorithm

$$\begin{cases} x_{a_j} = X_{a_j}\cos(B_{a_j}) + L\cos(A_{a_j})\sin(B_{a_j}) + Z_{a_j}\cos(A_{a_j})\sin(B_{a_j}) + Y_{a_j}\sin(A_{a_j})\sin(B_{a_j}) \\ y_{a_j} = Y_{a_j}\cos(A_{a_j}) - L\sin(A_{a_j}) - Z_{a_j}\sin(A_{a_j}) \\ z_{a_j} = X_{a_j}\sin(B_{a_j}) - Z_a\cos(A_{a_j})\cos(B_{a_j}) - Y_{a_j}\cos(A_{a_j})\sin(B_{a_j}) - L\cos(A_{a_j})\cos(B_{a_j}) \end{cases} \tag{17}$$

According to the definition of the contouring error, the normal deviation of the actual tool tip position from the ideal tool tip path is:

$$\varepsilon = [\varepsilon_x, \varepsilon_y, \varepsilon_z] = P_n - P_a = [x_n - x_a, y_n - y_a, z_n - z_a] \tag{18}$$

where $P_n = [x_n, y_n, z_n]$ is the nearest point on the transformed ideal tool tip path.

As shown in Fig. 10, the ND-contouring error is the normal deviation of the actual tool tip position from the transformed ideal tool path.

$$P_{t_\tau}^{(\tau)} = M^{(\tau)} \left[\prod_{u=n, L^u(4)=0}^{u=1} T_{L^u(4)L^{u-1}(4)}^{(\tau)} \right]^{-1} \left[\prod_{t=n, L^n(8)=0}^{t=1} T_{L^t(8)L^{t-1}(8)}^{(\tau)} \right] \cdot P_T \tag{19}$$

$$\varepsilon_\tau = P_{a_\tau} - P_{n_\tau}^{(\tau)} = \left[x_{a_\tau} - x_{n_j}{}^{(\tau)}, y_{a_\tau} - y_{n_j}{}^{(\tau)}, z_{a_\tau} - z_{n_j}{}^{(\tau)} \right] \tag{20}$$

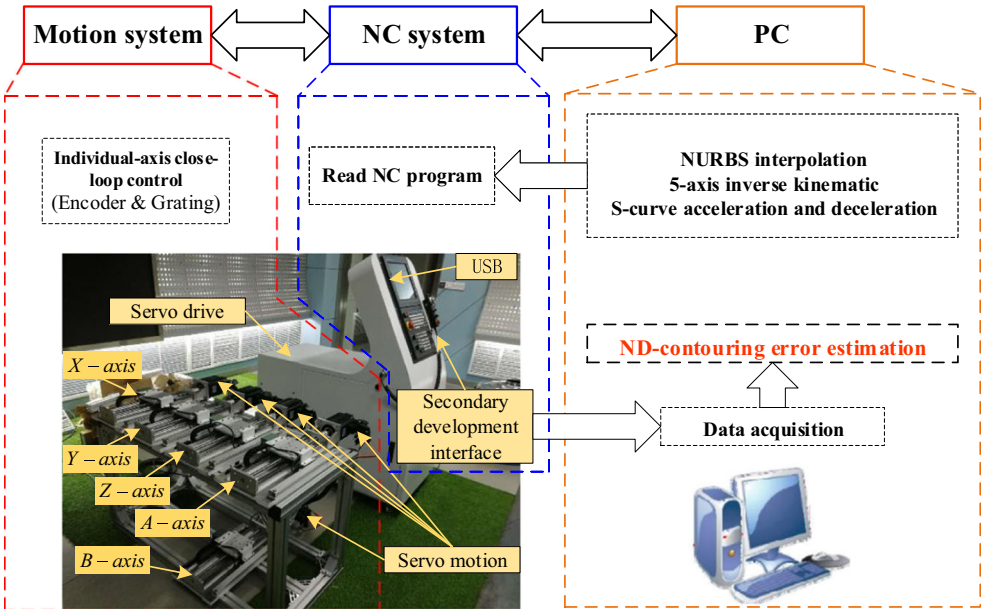

Fig. 14 Virtual five-axis machine tool used in the experiments

Here, $P_{t_\tau}^{(\tau)} = M^{(\tau)} P'_{i_\tau}$ is the current ideal position P'_{i_τ} on the transformed ideal tool path in the workpiece coordinate system, and P_{n_τ} is the nearest point on the transformed ideal tool path in the vicinity of the actual point position.

In the process of densifying the sampling ideal tool tip points by NURBS curve interpolation, the ideal tool path is transformed by line segments, which have enough accuracy to represent the original reference tool path. Thus, at the first step, the nearest position $P_{t_j}^{(\tau)}$ relative to the actual point can be found using the following formula.

$$P_{t_j}^{(\tau)} = \text{argmin}_{j=0,1,\ldots\tau} \| P_{t_j}^{(\tau)} - P_{a_\tau} \| \tag{21}$$

Then, three cases may occur, and the definitions of contouring error in each case are shown in Fig. 11.

After the nearest tool tip position $P_{n_\tau} = \left[x_{n_\tau}, y_{n_\tau}, z_{n_\tau}\right]^T$ is obtained, the tool orientation contour error ε_{O_τ} is defined as the angular orientation difference between $O_{a_\tau} = \left[i_{a_\tau}, j_{a_\tau}, k_{a_\tau}\right]$ and $O_{n_\tau} = \left[i_{n_\tau}, j_{n_\tau}, k_{n_\tau}\right]$. The definition of tool orientation contouring errors is shown in Fig. 12.

The ND-contouring error of tool tip and tool orientation is conducted as follows:

$$\begin{aligned} \Delta_\tau &= \|\varepsilon_\tau\| = \|P_{a_\tau}^{(\tau)} - P_{n_\tau}\| = \left(P_{a_\tau}^{(\tau)} - P_{n_\tau}\right)^T \left(P_{a_\tau}^{(\tau)} - P_{n_\tau}\right) \\ &= \sqrt{\left(x_{a_j}{}^{(\tau)} - x_{n_\tau}\right)^2 + \left(y_{a_j}{}^{(\tau)} - y_{n_\tau}\right)^2 + \left(z_{a_j}{}^{(\tau)} - z_{n_\tau}\right)^2} \end{aligned} \tag{22}$$

$$\begin{aligned} \Delta_{O_\tau} &= \|\varepsilon_{O_\tau}\| = \|O_{a_\tau}^{(\tau)} - O_{n_\tau}\| \\ &= \left(O_{a_\tau}^{(\tau)} - O_{n_\tau}\right)^T \left(O_{a_\tau}^{(\tau)} - O_{n_\tau}\right) \\ &= \sqrt{\left(i_{a_j}{}^{(\tau)} - i_{n_\tau}\right)^2 + \left(j_{a_j}{}^{(\tau)} - j_{n_\tau}\right)^2 + \left(k_{a_j}{}^{(\tau)} - k_{n_\tau}\right)^2} \end{aligned} \tag{23}$$

Combined with the registration of the free-form tool tip path in Section 3.1, the integrated flowchart of the ND-contouring error estimation algorithm is shown in Fig. 13. The actual tool tip position and tool orientation in the workpiece frame are calculated from the homogeneous matrix transformation. The ideal tool tip points are densified by NURBS curve interpolation. To achieve sufficiently accuracy to represent the original ideal tool path, the discrepancy

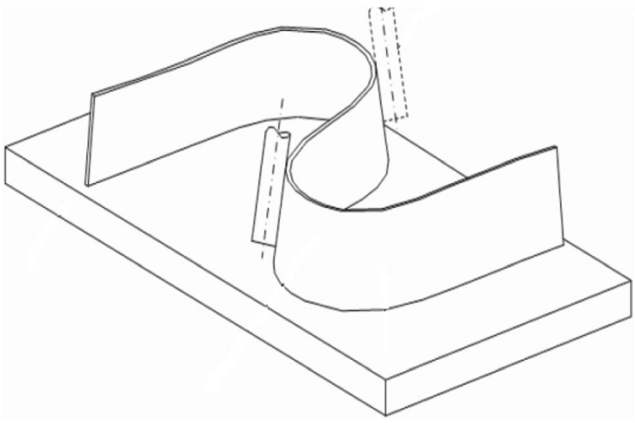

Fig. 15 S test piece

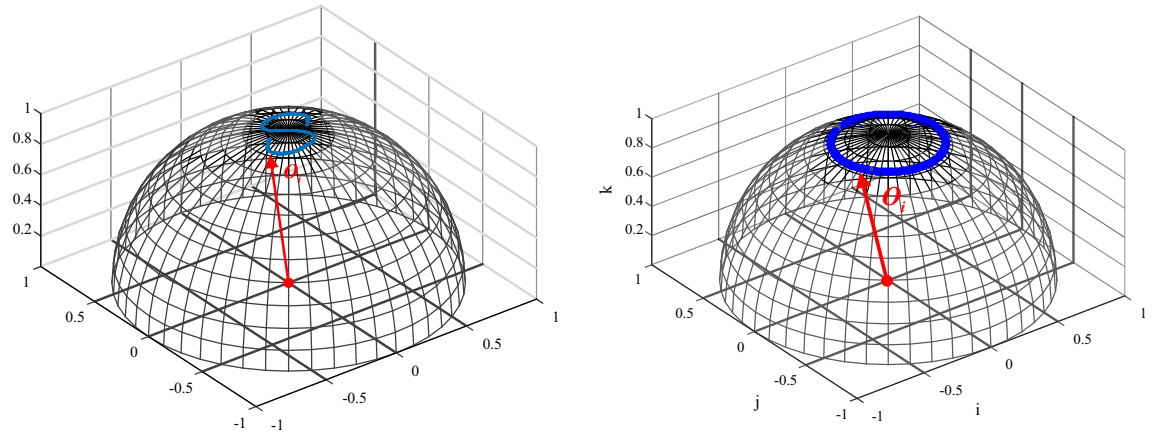

(a) S-path (b) B-path

Fig. 16 The tool orientation paths of **a** S-path and **b** B-path in the sphere coordinate

between the interpolated short line segments and the ideal tool tip path is limited to the preset chord error tolerance δ_{max}. The closest points corresponding to each actual tool tip point are searched from the densified ideal tool tip points. Subsequently, the actual tool tip points and their corresponding ideal tool tip points are matched, and the matching transformation is calculated by minimizing the maximum distances of the collective point-to-point. Finally, the ND-contouring error is estimated by calculating the minimum distance of the actual tool tip and the transformed ideal tool tip path, and the tool orientation contour error is estimated by calculating the difference between the actual tool orientation and the tool orientation at the nearest tool tip point.

4 Simulation and experiment

4.1 Verification of the contouring error estimation accuracy

The proposed five-axis ND-contouring error estimation method is verified on a five-axis experimental platform with the HNC control system (Fig. 14). Each axis has independent closed-loop control through the encoder and grating ruler. Although the platform is different from the real five-axis machine tool, the platform does not influence the verification of the proposed ND-contouring error estimation algorithm. Three translational movements are achieved by using a ball screw, while the two rotary axes are not assembled to the machine body. The platform does not affect the verification of the proposed contour error estimation algorithm, although the experiment platform in the study is slightly different to a real five-axis machine because the ND-contouring error calculation is essentially a geometric issue [18]. In addition, as we know, for a real five-axis machine tool, there are many factors that can cause position errors for the tool tip point, such as the contouring error, the quasi-static geometric error, and the dynamic geometric error [31]. It is difficult to know how much tool tip error of a real five-axis machine tool is affected by the contouring error. Thus, it is reasonable to verify the accuracy of the proposed estimation algorithm using this experimental platform.

In the experiment, the NC program is input to the CNC system via the USB interface. The S-curve acceleration and

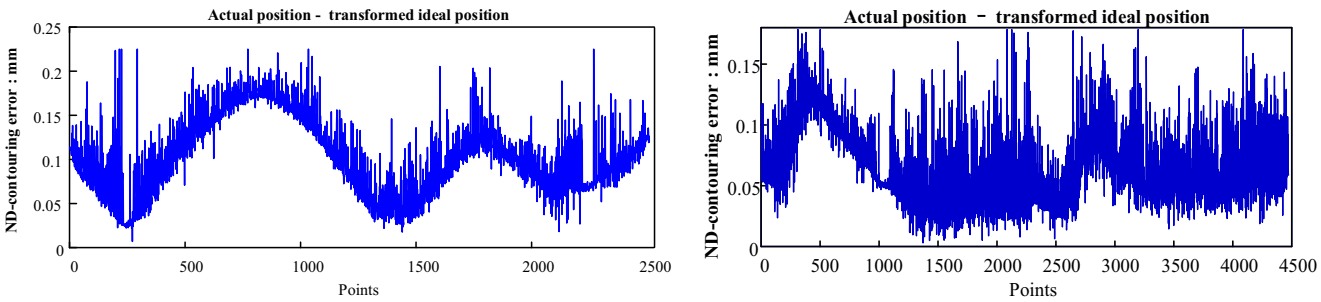

(a) S-path (b) B-path

Fig. 17 Experimental results of the tool tip position ND-contouring error for the **a** S-path and **b** B-path

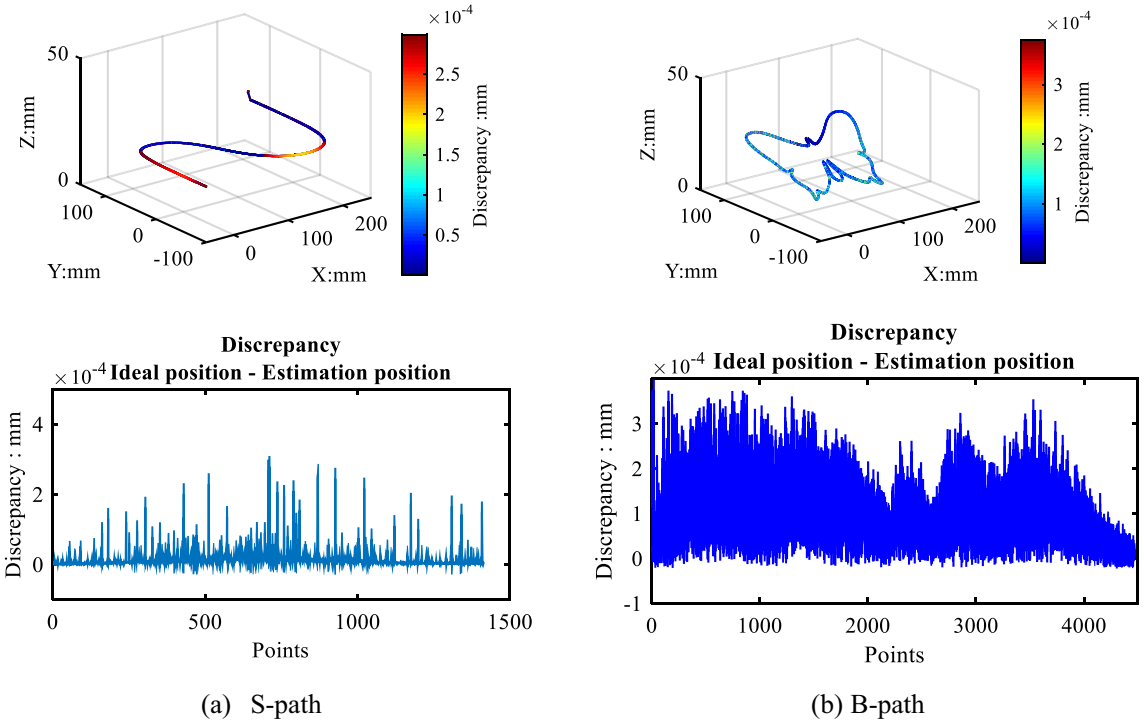

(a) S-path (b) B-path

Fig. 18 The estimated tool tip position splines and their discrepancy with the ideal positions for the **a** S-path and **b** B-path

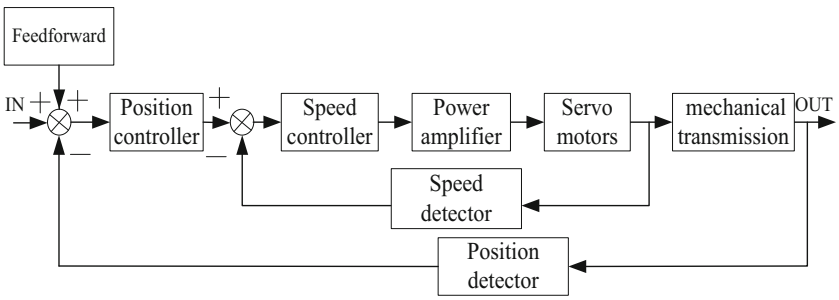

Fig. 19 Servo system block diagram

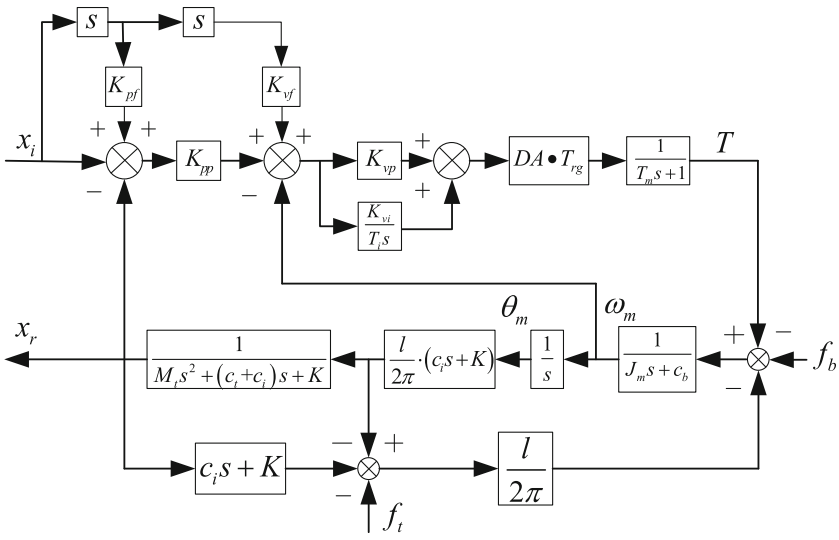

Fig. 20 Servo system of the translation axis

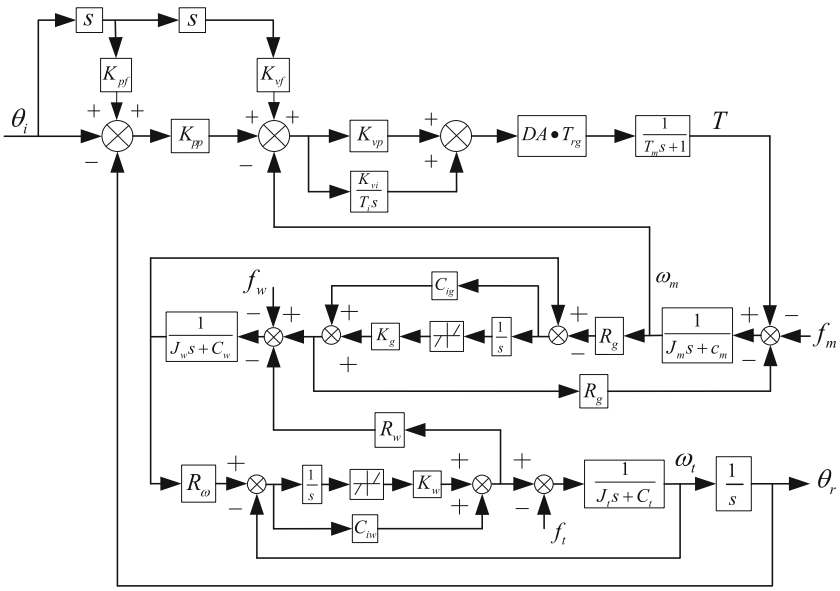

Fig. 21 Servo system for the rotation axis

deceleration method is applied in the drive control. The maximum velocity constraint is 250 mm/s, and the maximum acceleration is ± 500 mm/s^2 for each axis. During the operation of the experimental platform, we collected the data in real time through the secondary development interface provided by Wuhan Huazhong Numerical Control Co., Ltd. (HNC). The data collected include actual positions and command positions of five drivers, and the actual positions are fed back by the grating ruler. The collected actual position and command position of five drives are defined in the machine coordinate system. The tool actual position P_a and the ideal position P_i in the workpiece frame are obtained by the HTM method and are then used in the proposed contouring error estimation algorithm.

Two representative trajectories are adopted to verify the proposed ND-contouring error estimation method. The first trajectory is the five-axis S tool path (S-path) [32]. The S-path is generated by the S test piece (ISO 10791-7) as shown in Fig. 15. The S test piece has obvious advantages to reflect the dynamic error such as servo mismatch, nonlinear error, reverse error, and poor rigidity of machine tools. The S test piece is used to identify the performance of a five-axis machine tool [33, 34].

The second trajectory is the five-axis butterfly-shaped tool path (B-path). The B-path used in this paper is obtained by making some adjustments to the butterfly-shaped trajectory in the reference [35]. The butterfly-shaped trajectory has various changes of curvature. The trajectory in the reference [35] is tilted 10° so that it becomes a three-dimensional tool tip path. For the tool orientation, the motion relational expression of the rotary axis A and B is as follows:

$$\begin{cases} A = \dfrac{\pi}{9}\sin(\omega t) \\ B = \dfrac{\pi}{9}\sin\left(\omega t + \dfrac{\pi}{2}\right) = \dfrac{\pi}{9}cos(\omega t) \\ \omega T = 2\pi \end{cases} \tag{24}$$

Table 1 Physical meaning of symbols

Symbol	Physical meaning	Symbol	Physical meaning
J_m	Moment of inertia of the motor	θ_m	Angular displacement of the motor
C_m	Damping coefficient of the motor	R_g	Gear ratio
T_g	Output torque of gear transmission	C_{ig}	Damping coefficient of between motor and gear transmission
f_m	Friction torque of the motor	T_m	Output torque of the motor
J_w	Moment of inertia of worm gear	θ_w	Angular displacement of worm gear
C_w	Damping coefficient of worm gear	R_w	Worm gear ratio
C_{iw}	Damping coefficient between the workbench and worm gear	J_t	Moment of inertia of workbench
θ_t	Angular displacement of workbench	C_t	Damping coefficient of workbench
f_t	Friction torque of workbench	T_w	Output torque of workbench

where T is the total time of the tool movement, and $t \in [0, T]$.The tool orientation paths of S-path and B-path in sphere coordinate are shown in Fig. 16.

The ND-contouring errors of the five-axis S-path and B-path are shown in Fig. 17. As the ND-contouring error in this paper is not related to a datum, the way to verify the efficiency of contouring error estimation in reference [18] that compared the estimated and actual contouring error is not applicable here. To test and verify the accuracy of the proposed five-axis contouring error estimation algorithm, an estimation tool tip position spline is obtained by adding the real-time estimated contouring error vector to the corresponding actual tool tip position. The estimated tool tip position spline can reflect the information of the estimated ND-contouring error. The object in this study is the form error of tool tip position spline, and the form error between the estimated and ideal tool tip position splines can reflect the accuracy of the estimation algorithm. The difference between the estimation trajectory and the ideal

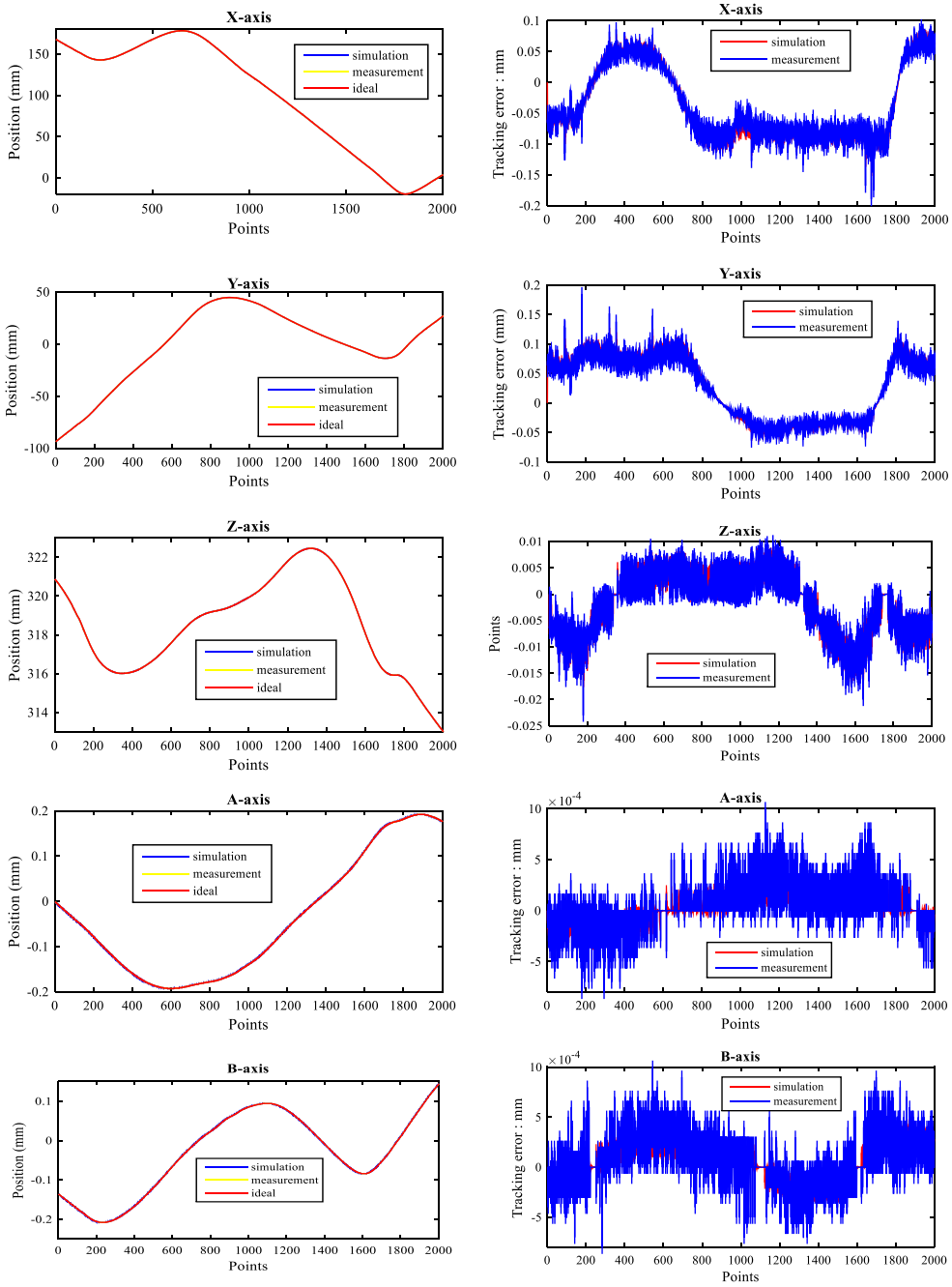

(a) Position response of each axis

(b) Tracking error of each axis

Fig. 22 **a** Position response and **b** tracking error of each axis

trajectory is negligibly small (Fig. 18), and their discrepancy is a few thousandths of the corresponding ND-contouring error. The distribution of the discrepancy values is shown in the chromatogram, and the size of the values is represented by different colors. The experimental results show that the discrepancy between the estimated and actual paths for S-path and B-path curve is less than 1 μm and 0.4 μm, respectively. The estimation accuracy of the proposed method is within an acceptable range of five-axis CNC machining.

4.2 Verification of the effectiveness of compensation based on the proposed ND-contouring error estimation

Since the ND-contouring errors have been estimated with high accuracy, ND-contouring error is controlled to verify the effectiveness of the proposed estimation method. The motion system model of each axis for a five-axis machine tool is first established. The translational and rotary axes have similar control systems [32] as shown in Fig. 19. By incorporating servo control links and mechanical transmission links, the whole virtual motion systems of the rotary axis and translational axis are established as displayed in Fig. 20 and Fig. 21, respectively (Table 1).

The virtual motion system and the real motion system are given the same command position. The actual positions of the five virtual feed drives are obtained by simulation. The actual positions of the real five-axis experimental platform are obtained by measurement. The command position, the actual position of simulation, and the measurement of each axis are shown in Fig. 22. The tracking errors of virtual motion system and the real motion system are placed in the same graph for easier comparison. It can be seen that the results of the virtual kinematic responses are close to those of the actual response.

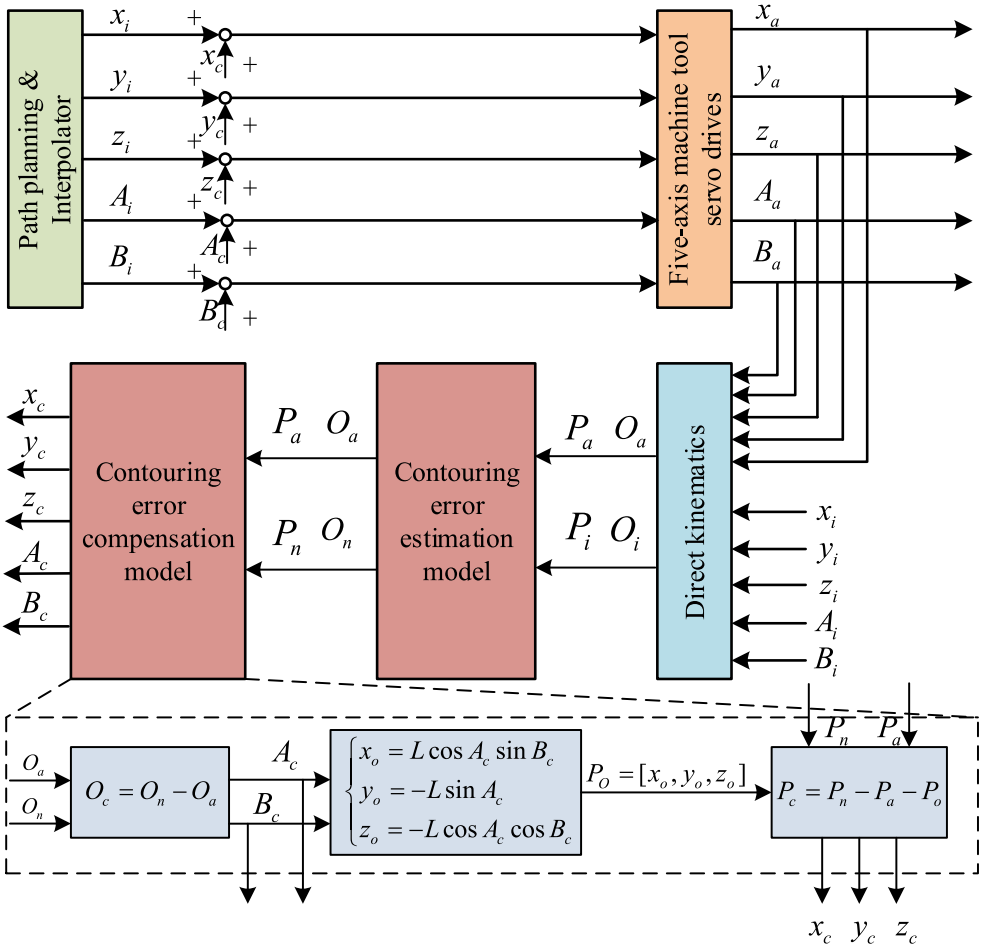

Fig. 23 Control structure of five-axis contouring error. x_i, y_i, z_i, A_i, B_i: Ideal commands of x, y, z, A, and B axes. x_a, y_a, z_a, A_a, B_a: Actual outputs of x, y, z, A, and B axes. x_c, y_c, z_c, A_c, B_c: Compensated commands of x, y, z, A, and B axes

x_i, y_i, z_i, A_i, B_i : Ideal commands of $x, y, z, A,$ and B axes

x_a, y_a, z_a, A_a, B_a : Actual outputs of $x, y, z, A,$ and B axes

x_c, y_c, z_c, A_c, B_c : Compensated commands of $x, y, z, A,$ and B axes

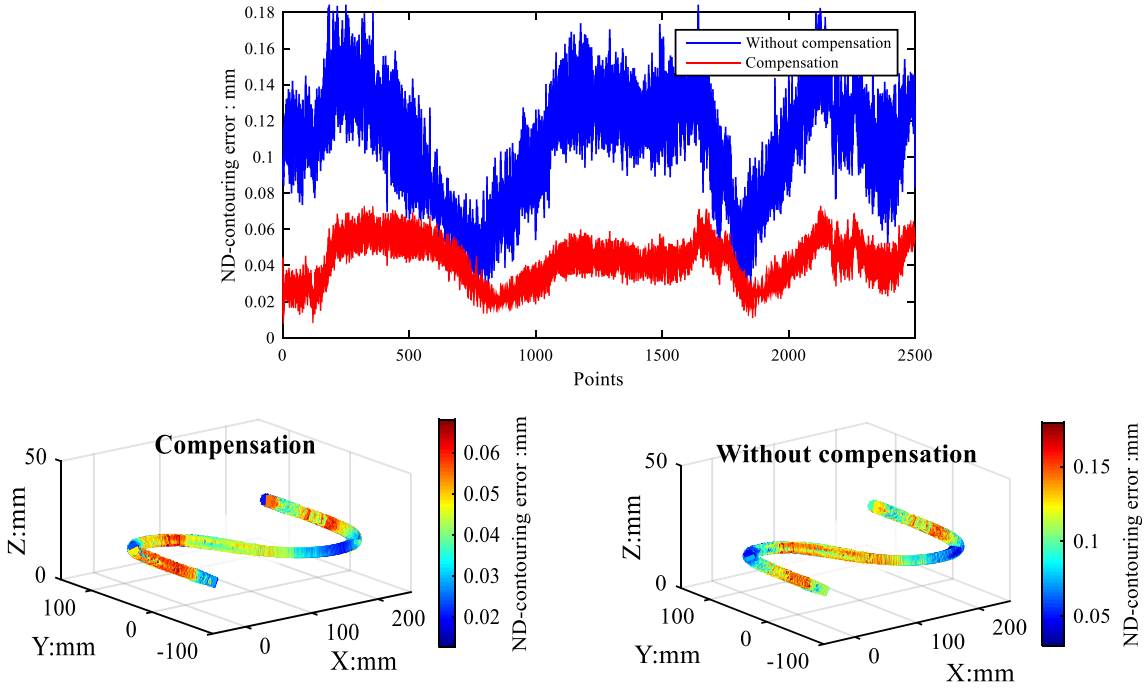

Fig. 24 Simulation results of tool tip position contouring error for the S-path

In the experiment of ND-contouring error control, it is reasonable to use the virtual motion system instead of the experimental platform for experiments.

The estimated five-axis ND-contouring error is controlled by the position loop of each drive axis [36] as shown in Fig. 23. According to the proposed ND-contouring error estimation algorithm, the nearest tool tip position and tool orientation are obtained. The nearest tool tip position and tool orientation are transformed to the position of each axis by inverse kinematic transformation. Then, the estimated ND-contouring error components on each drive are compensated to the position commands of the corresponding drive. The ND-contouring error during five-axis following of the S-path and B-path are resimulated. As illustrated in Fig. 24 and

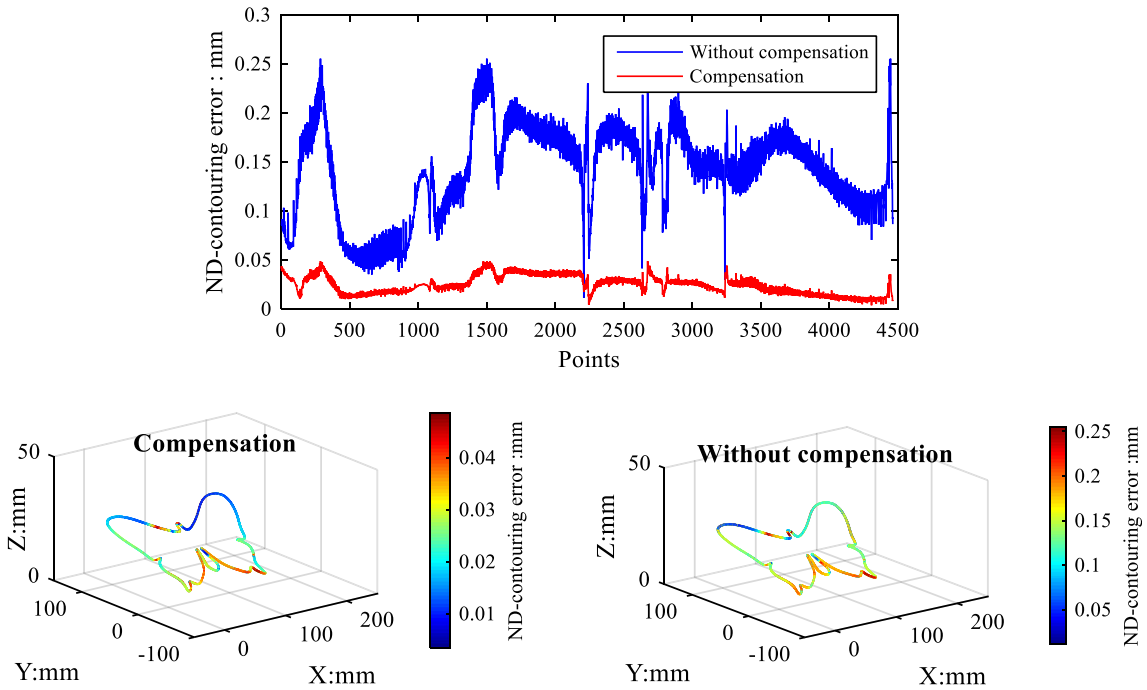

Fig. 25 Simulation results of tool tip position contouring error for the B-path

Table 2 Comparison of ND-contouring errors with and without compensation based on the proposed contouring error estimation algorithm

	S-path		B-path	
	MAX (mm)	RMS (mm)	MAX (mm)	RMS (mm)
Uncompensated	0.1793	0.1120	0.2551	0.1489
Compensated	0.0681	0.0436	0.0486	0.0261
(1 − Compensated/Uncompensated) × 100%	62.03%	61.07%	80.96%	82.47%

Fig. 25, the ND-contouring errors of the S-path and B-path are both significantly reduced compared with the original ND-contouring error. Specifically, as presented in Table 2, the MAX and RMS values of the S-path are reduced by 62.03% and 61.07%, respectively. The MAX and RMS values of the B-path are reduced by 80.96% and 82.47%, respectively. Hence, the proposed ND-contouring error estimation algorithm can be effectively adopted for ND-contouring error control to improve the five-axis CNC machine tool machining accuracy.

5 Conclusions

Contouring error is a critical concern that affects the machining accuracy of high-performance parts with complex curved surfaces. The estimation accuracy of contouring error will also impact the error compensation effect of a machine tool, which will ultimately affect the quality of parts. Previously presented contouring error estimation methods focus on the reduction of the position error of the path to obtain better position accuracy of parts. Unlike previous estimation methods, this paper presents an ND-contouring error estimation algorithm focusing on the form error requirements. The ideal tool tip path has been transformed to match the actual one using the MZT method, and the ND-contouring error and orientation contouring error of a tool were estimated based on the transformed ideal tool path. Compared with previous contouring error, the proposed ND-contouring error obtains better form accuracy. The extensive simulation and experimental results demonstrate that the proposed multi-axis ND-contouring error estimation method is effective and accurate.

Funding information This work is supported by the National Key Scientific and Technological Project (Grant No. 2015ZX04001002).

References

1. Erkorkmaz K, Altintas Y (2001) High speed CNC system design. Part III: high speed tracking and contouring control of feed drives. Int J Mach Tools Manuf 41(11):1637–1658
2. Huo F, Poo AN (2013) Precision contouring control of machine tools. Int J Adv Manuf Technol 64(1–4):319–333
3. Jia ZY, Ma JW, Song DN, Wang FJ, Liu W (2018) A review of contouring-error reduction method in multi-axis CNC machining. Int J Mach Tools Manuf 125:34–54
4. Tung ED, Tomizuka M (1993) Feedforward tracking controller design based on the identification of low frequency dynamics. J Dyn Syst Meas Control 115(3):348–356
5. Ruderman M (2014) Tracking control of motor drives using feedforward friction observer. IEEE Trans Ind Electron 61(7): 3727–3735
6. Tomizuka M (1987) Zero phase error tracking algorithm for digital control. J Dyn Syst Meas Control 109(1):65–68
7. Altintas Y, Erkorkmaz K, Zhu WH (2000) Sliding mode controller design for high speed feed drives. CIRP Ann Manuf Technol 49: 265–270
8. Ramesh R, Mannan MA, Poo AN (2005) Tracking and contour error control in CNC servo systems. Int J Mach Tools Manuf 45(3):301–326
9. Koren Y (1980) Cross-coupled biaxial computer control for manufacturing systems. J Dyn Syst Meas Control 102:265–272
10. Yang J, Zhang HT, Ding H (2017) Contouring error control of the tool center point function for five-axis machine tools based on model predictive control. Int J Adv Manuf Technol 88(9–12): 2909–2919
11. Zhang D, Chen Y, Chen Y (2016) Iterative pre-compensation scheme of tracking error for contouring error reduction. Int J Adv Manuf Technol 87(9–12):3279–3288
12. Lo C, Chung C (1999) Tangential-contouring controller for biaxial motion control. J Dyn Syst Meas Control-Trans ASME 121:126–129
13. Yang J, Li Z (2011) A novel contour error estimation for position loop-based cross-coupled control. IEEE-ASME Trans Mechatron 16(4):643–655
14. Lou Y, Meng H, Yang JZ, Li ZX, Gao J, Chen X (2014) Task polar coordinate frame-based contouring control of biaxial systems. IEEE Trans Ind Electron 61(7):3490–3501
15. Liu W, Sun Y, Yuan X, Chen M (2017) A new approach to the pre-compensation of contour errorsfor three-axis machine tools using an adaptive cross-coupled controller. Int J Adv Manuf Technol 90(9–12):3711–3725
16. Hu C, Yao B, Wang Q (2011) Global task coordinate frame-based contouring control of linear-motor-driven biaxial systems with accurate parameter estimations. IEEE Trans Ind Electron 58(11): 5195–5205
17. Li X, Zhao H, Zhao X, Ding H (2016) Dual sliding mode contouring control with high accuracy contour error estimation for five-axis CNC machine tools. Int J Mach Tools Manuf 108: 74–82
18. Yang J, Ding H, Zhao H, Yan S (2016) A generalized online estimation algorithm of multi-axis contouring errors for CNC machine tools with rotary axes. Int J Adv Manuf Technol 84(5–8):1239–1251
19. Yang M, Yang J, Ding H (2018) A high accuracy on-line estimation algorithm of five-axis contouring errors based on three-point arc approximation. Int J Mach Tools Manuf 130–131:73–84

20. Pi S, Liu Q, Liu Q (2018) A novel dynamic contour error estimation and control in high-speed CNC. Int J Adv Manuf Technol 96(1433–3015):547–560
21. Rossi A, Lanzetta M (2013) Optimal blind sampling strategy for minimum zone roundness evaluation by metaheuristics. Precis Eng 37(2):241–247
22. International Standards Organization (ISO) (2012) ISO 1101-18: geometrical product specification (GPS) —geometrical tolerances — tolerances of form, orientation, location and run-out, Part 18: definitions of geometrical tolerances
23. Zhang Z (1994) Iterative point matching for registration of free-form curves and surfaces. Int J Comput Vis 13(2):119–152
24. Yu DP, Hong GS, Wong YS (2012) Profile error compensation in fast tool servo diamond turning of micro-structured surfaces. Int J Mach Tools Manuf 52(1):13–23
25. Zhang X, Jiang X, Scott PJ (2011) A reliable method of minimum zone evaluation of cylindricity and conicity from coordinate measurement data. Precis Eng 35(3):484–489
26. The American society of mechanical engineers (ASME) (2012) ASME Y 14.4.1M-2012: digital product definition data practices
27. Lin MT, Tsai MS, Yau HT (2007) Development of a dynamics-based NURBS interpolator with real-time look-ahead algorithm. Int J Mach Tools Manuf 47(15):2246–2262
28. Zhang XT, Song Z (2012) An iterative feedrate optimization method for real-time NURBS interpolator. Int J Adv Manuf Technol 62(9–12):1273–1280
29. Zhang K, Yuan CM, Gao XS (2013) Efficient algorithm for time-optimal feedrate planning and smoothing with confined chord error and acceleration. Int J Adv Manuf Technol 66(9–12):1685–1697
30. Cheung CF, Li H, Kong L, Lee LB, To S (2006) Measuring ultra-precision freeform surfaces using a robust form characterization method. Meas Sci Technol 17(3):488–494
31. Andolfatto L, Lavernhe S, Mayer JRR (2011) Evaluation of servo, geometric and dynamic error sources on five-axis high-speed machine tool. Int J Mach Tools Manuf 51(10–11):787–796
32. Jiang Z, Ding JX, Song ZY, Du L, Wang W (2016) Modeling and simulation of surface morphology abnormality of 'S' test piece machined by five-axis CNC machine tool. Int J Adv Manuf Technol 85(9–12):2745–2759
33. Wang W, Jiang Z, Tao W, Zhuang W (2015) A new test part to identify performance of five-axis machine tool—part I: geometrical and kinematic characteristics of S part. Int J Adv Manuf Technol 79(5–8):729–738
34. Wang W, Jiang Z, Li Q, Tao W (2015) A new test part to identify performance of five-axis machine tool-part II validation of S part. Int J Adv Manuf Technol 79(5–8):739–756
35. Yang S, Ghasemi AH, Lu X, Okwudire CE (2015) Pre-compensation of servo contour errors using a model predictive control framework. Int J Mach Tools Manuf 98:50–60
36. Yang J, Altintas Y (2015) A generalized on-line estimation and control of five-axis contouring errors of CNC machine tools. Int J Mach Tools Manuf 88:9–23